CHALMERS

Internal Report 03/01

NATURAL CONVECTION HEAT TRANSFER IN A VERTICAL SHELL AND TUBE

Darioush G. Barhaghi, Lars Davidson, Rolf Karlsson

Department of Thermo and Fluid Dynamics
CHALMERS UNIVERSITY OF TECHNOLOGY
Göteborg, Sweden, December 2002

NATURAL CONVECTION HEAT TRANSFER IN A VERTICAL SHELL AND TUBE

Darioush Gohari Barhaghi, Lars Davidson, Rolf Karlsson
Dept. of Thermo and Fluid Dynamics
Chalmers University of Technology
SE-412 96 Göteborg, Sweden

Contents

Abstract

Natural convection heat transfer and the resulting fluid flow in an experimental vertical shell and tube, implementing different turbulence models is studied. Different operating conditions of the facility to find the optimum condition are implemented and the effect of geometry simplifications on the predicted boundary layer is discussed. Also, the effect of different geometrical dimensions on the developed thermal and velocity boundary layers is shown.

Nomenclature

Latin Symbols

$C_{\varepsilon 1}, C_{\varepsilon 2}$	turbulence model constants
C_k, C_μ	turbulence model constants
$C_\omega, C_{\omega 1}, C_{\omega 2}$	turbulence model constants
c_p	fluid specific heat at constant pressure
$\hat{e}_r$	unit vector in r-direction
$\hat{e}_z$	unit vector in z-direction
$f_\varepsilon, f_k, f_\mu$	turbulence model damping functions
g_r	gravitational acceleration in r-direction
g_z	gravitational acceleration in z-direction
H	height of the shell and tube and the cavity
h	convection heat transfer coefficient
k	turbulence kinetic energy; fluid thermal conductivity
n	distance from the wall
P_k	turbulence production
Pr_t	turbulent Prandtl number, $(= 0.9)$
p	pressure
q_w	wall heat flux, $-k\partial T/\partial n$
R_i	hot tube radius
R_o	shell radius
r	distance in radial direction perpendicular to tube
r^+	dimensionless distance from wall, $v^*(r - R_i)/\nu$
r_v	velocity boundary layer thickness
r_T	thermal boundary layer thickness
S	clockwise distance from southwest corner
T	temperature
T_f	film temperature, $(T_h[K] + T_c[K])/2$
T^+	dimensionless temperature, $(T_w - T)/t^*$
t^*	friction temperature, $q_w/(\rho c_p v^*)$
U_o	buoyant velocity, $\sqrt{g\beta(T_h - T_c)H}$
v	vertical velocity in Cartesian coordinate system
v^+	dimensionless velocity, v_z/v^*
v^*	friction velocity, $\sqrt{\tau_w/\rho}$
$\mathbf{V}$	velocity vector, $v_r\hat{e}_r + v_z\hat{e}_z$

v_r	velocity component in r-direction
v_z	velocity component in z-direction
W	width of the cavity
x	Cartesian coordinate horizontal axis
y	Cartesian coordinate vertical axis
z	cylindrical coordinate vertical axis

Greek Symbols

α	thermal diffusivity, $k/(\rho c_p)$
β	coefficient of expansion, $1/T_f[K]$
ε	turbulence dissipation rate
μ	fluid dynamic viscosity
∇	gradient vector, $\frac{\partial}{\partial r}\hat{e}_r + \frac{\partial}{\partial z}\hat{e}_z$
ν_{eff}	effective kinematic viscosity
ν_t	turbulent kinematic viscosity
ω	specific dissipation, $\varepsilon/(0.09k)$
ρ	fluid density
$\sigma_\varepsilon, \sigma_k, \sigma_\omega$	turbulence model constants
τ_w	wall shear stress, $\mu\partial v_z/\partial n$
θ	azimuthal angle in cylindrical coordinate system

Dimensionless quantities

C_f	friction coefficient, $\tau_w/(\rho U_o^2/2)$
Gr_z	local Grashof number, $g\beta(T_w - T_\infty)z^3/\nu^2$
Nu	Nusselt number, $-H(\partial T/\partial n)_w/(T_h - T_c)$
Nu_z	local Nusselt number, $-z(\partial T/\partial n)_w/(T_h - T_c)$
Pr	Prandtl number, ν/α
Ra_z	local Rayleigh number, $g\beta(T_w - T_\infty)z^3/(\nu\alpha)$

Subscript

c	cold
h	hot
w	wall
∞	ambient

1 Introduction

Natural convection heat transfer, has always been of particular interest among heat transfer problems. In natural convection, fluid motion is caused by density variations resulting from temperature distribution. Many experimental studies have been performed during the last three decades and interesting results have been presented. Experiments of the turbulent boundary layer in air were conducted by Warner & Arpaci (1968) and Cheesewright (1968). The turbulent natural convection boundary layer along a vertical flat plate was studied by Tsuji & Nagano (1988). Turbulent natural convection around a heated vertical slender cylinder was studied by Persson & Karlsson (1996) and new turbulent structures were presented for the near wall region. Also, low turbulence natural convection in an air filled square cavity was studied by Tian & Karayiannis (2000) and very useful data on flow and thermal fields were presented. The Large Eddy Simulation (hereafter LES) of turbulent buoyant flow in a confined cavity was also studied by Peng & Davidson (2001), and the results of a dynamic model were compared to existing experimental results. The motivation for this numerical work is that new, detailed experimental data will soon be available from an experimental shell and tube rig which is designed to study the natural convection heat transfer from a vertical cylinder. It is also hoped that the computations can give some insight on how the test rig will work and thus aid us to modify and improve the rig design. Figure 1 shows the shell and tube and its geometrical dimensions schematically. The reason for choosing such a geometrical configuration is that although an idealized vertical natural convection boundary layer takes place in infinite surroundings, it is impossible to achieve such an ideal condition either in experiments or in numerical calculations for both experiments and calculations are very sensitive to the location of the infinite boundaries and any disturbances there (Persson & Karlsson, 1996). Another advantage of this geometrical configuration is that it makes it possible to create a truly two dimensional fluid flow and heat transfer. Despite the fact that the boundary layer along the hot tube is not a pure natural convection boundary layer, a great advantage is that all of boundary conditions are known and well defined.

Before performing the experiments and LES, it is practical to have

some knowledge about the operating conditions of the facility. Thus, before performing LES, which is very CPU work consuming, the different operating conditions of this rig is numerically simulated, using two dimensional Reynolds Averaged Navier Stokes (RANS) equations.

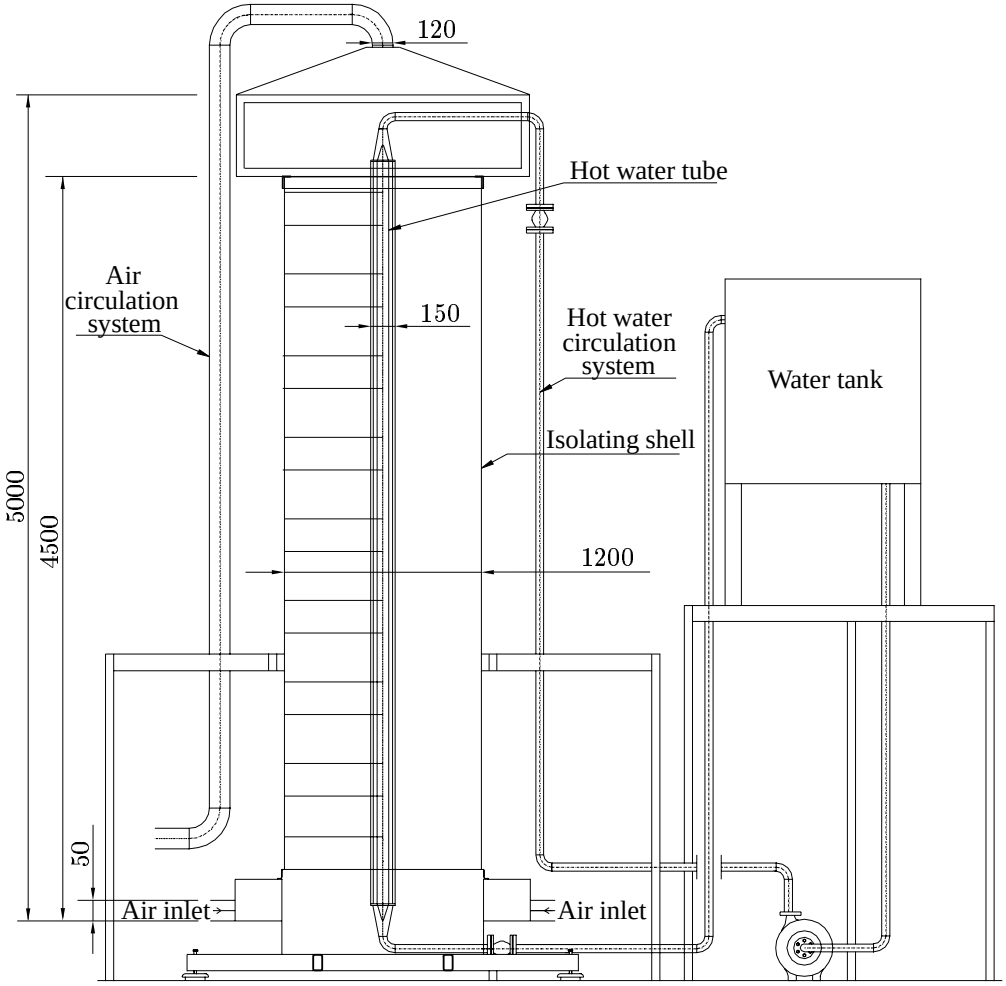

Figure 1: Experimental rig

During the operation, inner tube temperature is kept at 80^oC which

yields a Grashof number equal to about $4.5 \cdot 10^{11}$ and a Rayleigh number about $3.2 \cdot 10^{11}$. To keep the outgoing flow of the rig smooth and uniform, a perforated plate at the height of 4.5m is used. Also, perforated plates are used at the inlet in order that a uniform inlet velocity profile to be achieved.

To simulate the turbulent flow, two different turbulence models are considered. These two models are based on $k-\omega$ and $k-\varepsilon$ models, which are just modified for near wall low Reynolds number region. As the applicability of these models should first be examined on similar and simple natural convection problems, they are first applied to a confined cavity where both experimental and LES data are available.

2 Governing equations

The governing equations for the flow inside the shell and tube are the time averaged two dimensional cylindrical continuity and Navier-Stokes equations in which the Reynolds stress terms are modeled by the help of turbulent kinetic energy and turbulent dissipation equations.

Continuity:

$$\frac{1}{r}\frac{\partial}{\partial r}(rv_r) + \frac{\partial}{\partial z}(v_z) = 0 \tag{1}$$

Convective time derivative:

$$\mathbf{V}\cdot\nabla = v_r\frac{\partial}{\partial r} + v_z\frac{\partial}{\partial z} \tag{2}$$

Laplacian operator:

$$\nabla^2 = \frac{1}{r}\frac{\partial}{\partial r}\left(r\frac{\partial}{\partial r}\right) + \frac{\partial^2}{\partial z^2} \tag{3}$$

The r-momentum equation:

$$\begin{aligned}\frac{\partial v_r}{\partial t} + (\mathbf{V}\cdot\nabla)\,v_r = -\frac{1}{\rho}\frac{\partial p}{\partial r} + g_r + \frac{1}{r}\frac{\partial}{\partial r}\left(r\nu_{eff,v}\frac{\partial v_r}{\partial r}\right) + \\ \frac{\partial}{\partial z}\left(\nu_{eff,v}\frac{\partial v_r}{\partial z}\right) - \nu_{eff,v}\frac{v_r}{r^2}\end{aligned} \tag{4}$$

The z-momentum equation:

$$\frac{\partial v_z}{\partial t} + (\mathbf{V}\cdot\nabla)\, v_z = -\frac{1}{\rho}\frac{\partial p}{\partial z} + g_z\beta(T - T_f) + \frac{1}{r}\frac{\partial}{\partial r}\left(r\nu_{eff,v}\frac{\partial v_z}{\partial r}\right) + \frac{\partial}{\partial z}\left(\nu_{eff,v}\frac{\partial v_z}{\partial z}\right) \tag{5}$$

The energy equation:

$$\frac{\partial T}{\partial t} + (\mathbf{V}\cdot\nabla)\, T = \frac{1}{r}\frac{\partial}{\partial r}\left(r\nu_{eff,T}\frac{\partial T}{\partial r}\right) + \frac{\partial}{\partial z}\left(\nu_{eff,T}\frac{\partial T}{\partial z}\right) \tag{6}$$

Here, the turbulent diffusive cross terms arising from $\frac{\partial}{\partial x_j}\left(\nu_{eff}\frac{\partial v_j}{\partial x_i}\right)$ in which v_j stands for velocity vector, are neglected. The two turbulence models which have been used are the $k-\varepsilon$ model which is proposed by Abe *et al.* (1994) (hereafter referred to AKN model) and $k-\omega$ model of Peng *et al.* (1997) (hereafter referred to PDH model). For the AKN model the kinetic energy and the dissipation rate of turbulence equations are:

$$\frac{\partial k}{\partial t} + (\mathbf{V}\cdot\nabla)\, k = \frac{1}{r}\frac{\partial}{\partial r}\left(r\nu_{eff,k}\frac{\partial k}{\partial r}\right) + \frac{\partial}{\partial z}\left(\nu_{eff,k}\frac{\partial k}{\partial z}\right) + P_k - \varepsilon \tag{7}$$

$$\frac{\partial \varepsilon}{\partial t} + (\mathbf{V}\cdot\nabla)\, \varepsilon = \frac{1}{r}\frac{\partial}{\partial r}\left(r\nu_{eff,\varepsilon}\frac{\partial \varepsilon}{\partial r}\right) + \frac{\partial}{\partial z}\left(\nu_{eff,\varepsilon}\frac{\partial \varepsilon}{\partial z}\right) + \frac{\varepsilon}{k}(C_{\varepsilon 1}P_k - C_{\varepsilon 2}f_\varepsilon\varepsilon) \tag{8}$$

where:

$$P_k = 2\nu_t\left[\left(\frac{\partial v_r}{\partial r}\right)^2 + \left(\frac{\partial v_z}{\partial z}\right)^2\right] + \nu_t\left(\frac{\partial v_r}{\partial z} + \frac{\partial v_z}{\partial r}\right)^2 + \nu_t\left(\frac{2}{r^2}v_r^2\right)$$

$$\nu_{eff,v} = \nu + \nu_t$$

$$\nu_{eff,T} = \frac{\nu}{Pr} + \frac{\nu_t}{Pr_t}$$

$$\nu_{eff,k} = \nu + \frac{\nu_t}{\sigma_k}$$

$$\nu_{eff,\varepsilon} = \nu + \frac{\nu_t}{\sigma_\varepsilon}$$

$$\nu_t = C_\mu f_\mu \frac{k^2}{\varepsilon}$$

$$f_\mu = \left\{1 - \exp\left(-\frac{y^*}{14}\right)\right\}^2 \left[1 + \frac{5}{R_t^{3/4}} \exp\left\{-\left(\frac{R_t}{200}\right)^2\right\}\right]$$

$$f_\varepsilon = \left\{1 - \exp\left(-\frac{y^*}{3.1}\right)\right\}^2 \left[1 - 0.3 \exp\left\{-\left(\frac{R_t}{6.5}\right)^2\right\}\right]$$

$$y^* = \frac{u_\varepsilon y}{\nu}, \quad u_\varepsilon = (\nu\varepsilon)^{1/4}, \quad R_t = \frac{k^2}{\nu\varepsilon}$$

$$C_\mu = 0.09, \quad \sigma_k = 1.4, \quad \sigma_\varepsilon = 1.4, \quad C_{\varepsilon 1} = 1.5, \quad C_{\varepsilon 2} = 1.9$$

The value of ε for wall adjacent nodes is set to $\varepsilon_w = 2\nu k / n^2$. For PDH model the kinetic energy and specific dissipation equations are:

$$\frac{\partial k}{\partial t} + (\mathbf{V} \cdot \nabla) k = \frac{1}{r}\frac{\partial}{\partial r}\left(r \nu_{eff,k} \frac{\partial k}{\partial r}\right) + \frac{\partial}{\partial z}\left(\nu_{eff,k} \frac{\partial k}{\partial z}\right) + P_k - C_k f_k \omega k \tag{9}$$

$$\frac{\partial \omega}{\partial t} + (\mathbf{V} \cdot \nabla) \omega = \frac{1}{r}\frac{\partial}{\partial r}\left(r \nu_{eff,\omega} \frac{\partial \omega}{\partial r}\right) + \frac{\partial}{\partial z}\left(\nu_{eff,\omega} \frac{\partial \omega}{\partial z}\right) + \frac{\omega}{k}(C_{\omega 1} f_\omega P_k - C_{\omega 2}\omega^2) + C_\omega \frac{\nu_t}{k}\left(\frac{\partial \omega}{\partial r}\frac{\partial \omega}{\partial r} + \frac{\partial \omega}{\partial z}\frac{\partial \omega}{\partial z}\right) \tag{10}$$

where the two last terms in ω-equation are cross diffusion terms and:

$$\nu_{eff,\omega} = \nu + \frac{\nu_t}{\sigma_\omega}$$

$$\nu_t = C_\mu f_\mu k/\omega$$

$$f_\mu = 0.025 + \left\{1 - \exp\left[-\left(\frac{R_t}{10}\right)^{3/4}\right]\right\}\left\{0.975 + \frac{0.001}{R_t}\exp\left[-\left(\frac{R_t}{200}\right)^2\right]\right\}$$

$$f_k = 1 - 0.722\exp\left[-\left(\frac{R_t}{10}\right)^4\right]$$

$$f_\omega = 1 + 4.3\exp\left[-\left(\frac{R_t}{1.5}\right)^{1/2}\right]$$

$$R_t = \frac{k}{\nu\omega}$$

$$C_\mu = 1.0, \quad C_k = 0.09, \quad C_{\omega 1} = 0.42, \quad C_{\omega 2} = 0.075, \quad C_\omega = 0.75$$

$$\sigma_k = 0.8, \quad \sigma_\omega = 1.35$$

Similar to previous model, wall adjacent nodes achieve a value equal to $\omega_w = 6\nu/(C_{\omega 2} n^2)$.

3 Numerical method

The governing equations are solved in steady state conditions and a third order QUICK scheme for momentum equations and second order Van Leer scheme for turbulence models are used to discretise the governing equations (Davidson & Farhanieh, 1995). In order to solve the discretized equations, the SIMPLEC algorithm together with Rhie and Chow interpolation are employed.

4 Turbulence model assessment

In order to assess the ability of both turbulence models in predicting the fluid flow and heat transfer of typical natural convection problems, the natural convection in a confined square cavity is considered, where both experimental (Tian & Karayiannis, 2000) and LES results (Peng & Davidson, 2001) exist. The cavity's left and right walls are hot and cold respectively with a temperature difference of 40^oC. The cavity Rayleigh number is about $1.58 \cdot 10^9$. The top and bottom walls of the cavity are highly conductive walls which give a temperature distribution along these walls. As the temperature distribution along these two conductive walls were not linear, the temperature boundary condition are taken directly from the experimental values and a 96×96 mesh has been used. Figures 2(a), 2(b) and 3 compare the streamlines of flow inside the cavity by different models.

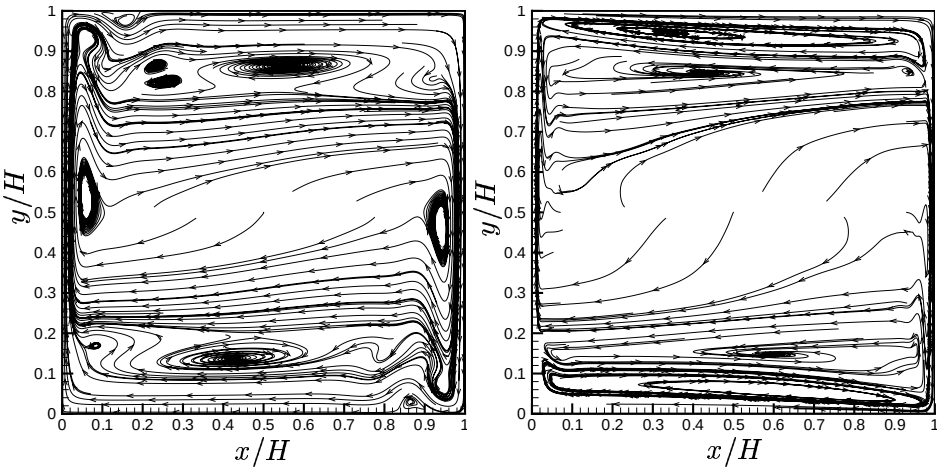

(a) $k-\omega$ (PDH) model

(b) $k-\varepsilon$ (AKN) model

Figure 2: RANS simulation

As it is obvious from the figures, the flow structure is predicted differently by different models. However, PDH model results look more alike LES model. Furthermore, by studying figure 4 it can be seen that the PDH model is generally in better agreement with experimental data.

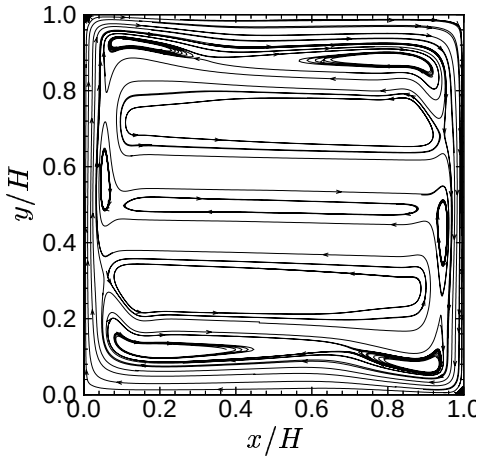

Figure 3: LES from Peng & Davidson (2001)

The reason for why the AKN model and the PDH model give different results is that the transition commencement is predicted differently by the two turbulence models.

5 Effect of inlet velocity

Among all, one of the most important boundary conditions that plays a vital role on the temperature stratification along the heated tube, is the inlet condition. The reason for this problem is depicted in figure 5.

If the rate of fluid flow inside the boundary layer approaching the outlet ($\dot{m}_{bl}$) becomes larger than the inlet flow rate ($\dot{m}_{in} = \dot{m}_{out}$), some part of fluid ($\dot{m}_{bl} - \dot{m}_{in}$) will recirculate in order to compensate this difference. The recirculating fluid brings hot fluid to the upper part of the domain. Thus, temperature stratification along the outer part of the boundary layer is inevitable, causing the boundary layer growth to be suppressed. However, by increasing the inlet flow rate, a smaller flow recirculation and consequently a smaller temperature stratification is likely to occur. Therefore, the aim is to apply an inlet flow rate large enough to reduce temperature stratification and small enough so that the natural convection remains the major phenomenon. So, different inlet velocities are applied and the effect of them are studied.

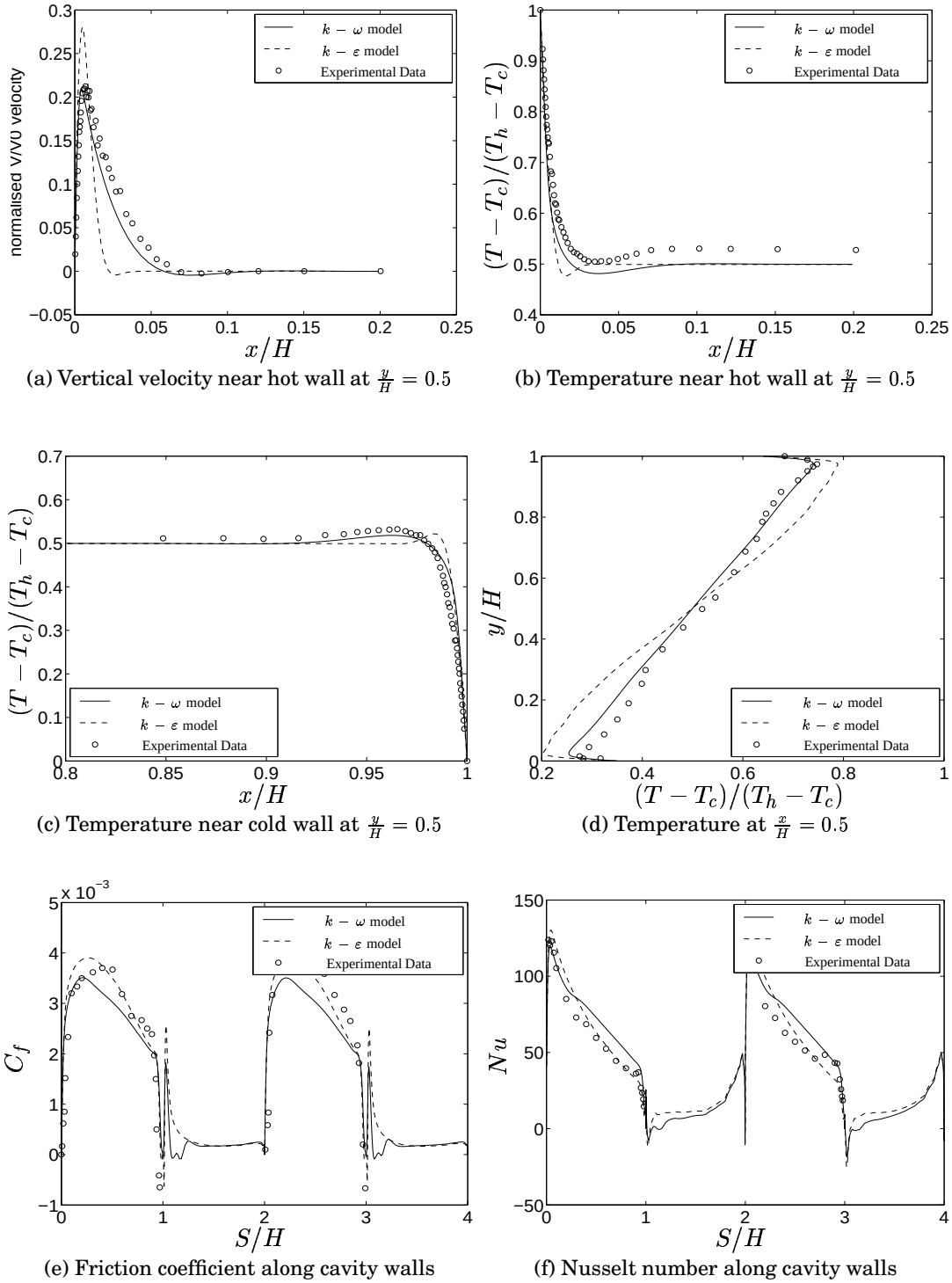

(a) Vertical velocity near hot wall at $\frac{y}{H} = 0.5$

(b) Temperature near hot wall at $\frac{y}{H} = 0.5$

(c) Temperature near cold wall at $\frac{y}{H} = 0.5$

(d) Temperature at $\frac{x}{H} = 0.5$

(e) Friction coefficient along cavity walls

(f) Nusselt number along cavity walls

Figure 4: Natural convection in a square cavity

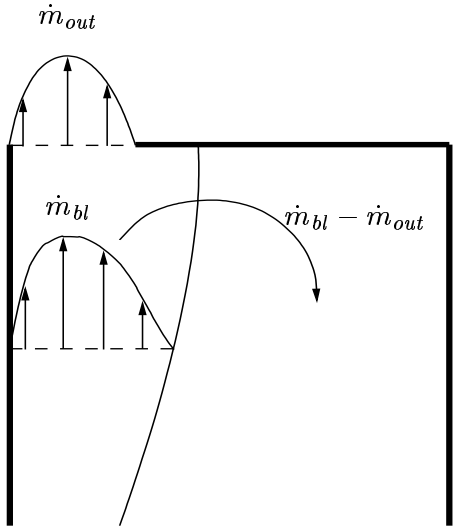

Figure 5: Temperature stratification due to recirculation

The computational geometry and boundary conditions are depicted in figure 6, in which all the dimensions are in millimeter. All the walls, except the hot tube which is shown thicker than the other walls, are considered as insulated walls and Neumann boundary condition for temperature is applied to them. The inlet flow is uniform and enters horizontally in the negative radial direction.

The effect of perforated plate is modeled in the calculations by regarding that the aspect ratio of *free area at plate* to *area of passage* of it is equal to 0.56. Considering this property, this plate gives a pressure drop equal to $\Delta p = K_o \rho v_z^2/2$ where $K_o = 3$ according to Miller (1990).

The calculations are carried out for three different inlet velocities equal to $0.4, 0.5$ and $0.6 m/s$ and PDH model is used. Figures 7(a) and 7(b) show thermal and velocity boundary layer developments. The thermal boundary layer is defined as where $(T_w - T)/(T_w - T_\infty) = 0.99$ and for velocity it is where the fluid velocity reaches to half of maximum fluid velocity.

Also, variation of local Nusselt number, Nu_z, is shown in figure 8 which shows a slightly earlier thermal transition commencement compared to flat plate around Rayleigh number equal to $5 \cdot 10^7$.

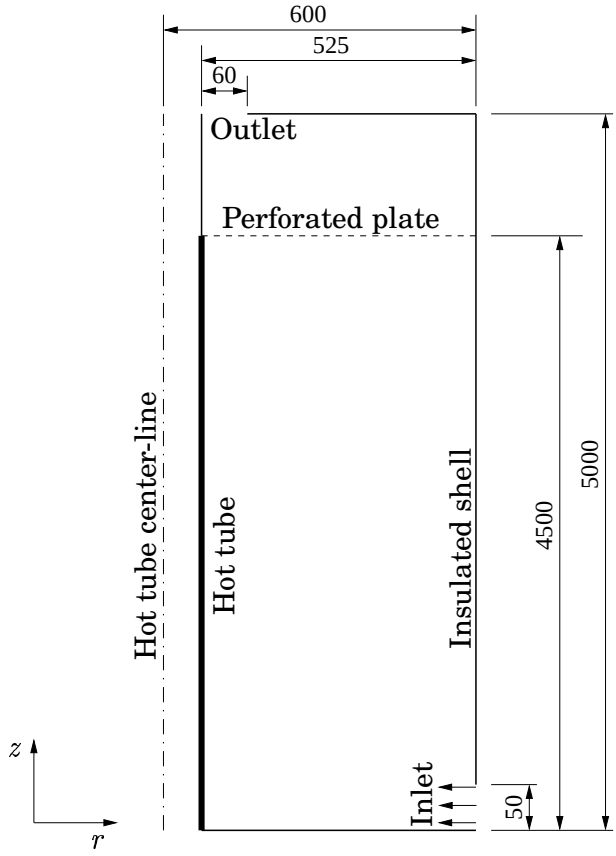

Figure 6: Computational geometry

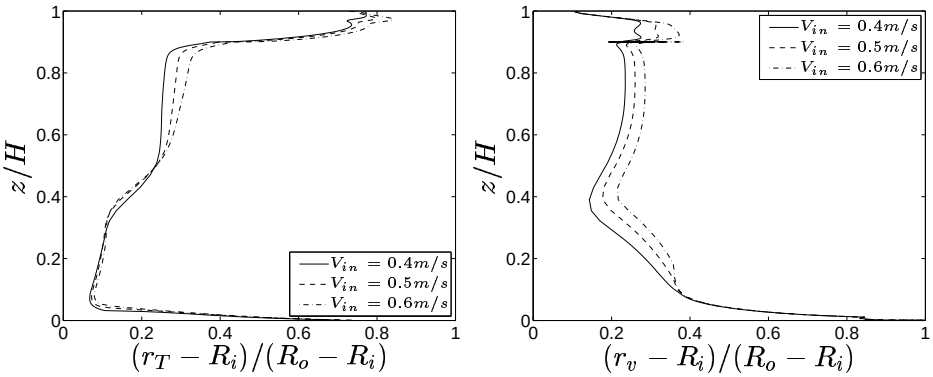

(a) thermal boundary layer (b) velocity boundary layer

Figure 7: Boundary layer growth for different inlet velocities

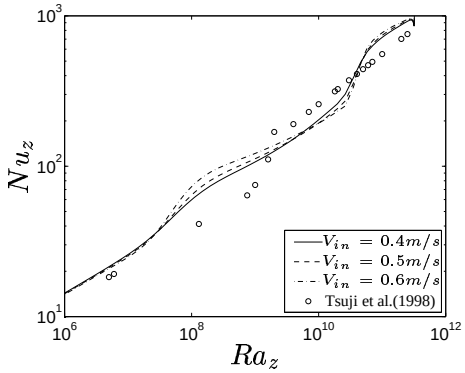

Figure 8: Heat transfer rate for different inlet velocities

In figure 9 the amount of temperature stratification along the shell and tube height at different radii for different inlet velocities are shown. From the figures, a larger temperature stratification for smaller inlet velocity is perceivable.

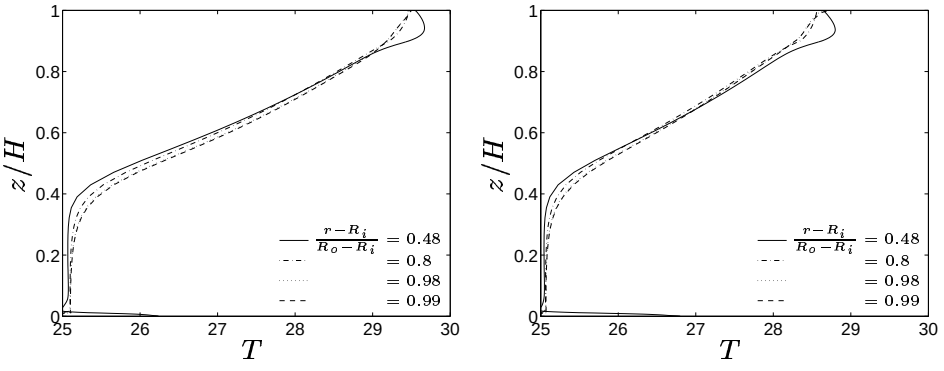

(a) $V_{in} = 0.4m/s$ (b) $V_{in} = 0.5m/s$

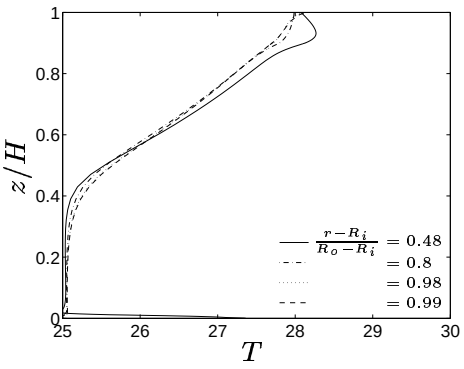

(c) $V_{in} = 0.6m/s$

Figure 9: Temperature stratification along shell height

6 Effect of perforated plate

For sake of simplicity it was of particular interest to investigate the effect of perforated plate and the possibility of elimination of it in the future LES simulations. Thus, a new geometry without perforated plate and a reduced $4.5m$ height and the same outlet was introduced. Figures 10(a) and 10(b) compare the thermal and velocity boundary layers growth of the two geometries with the inlet velocity (V_{in}) equal to $0.6m/s$.

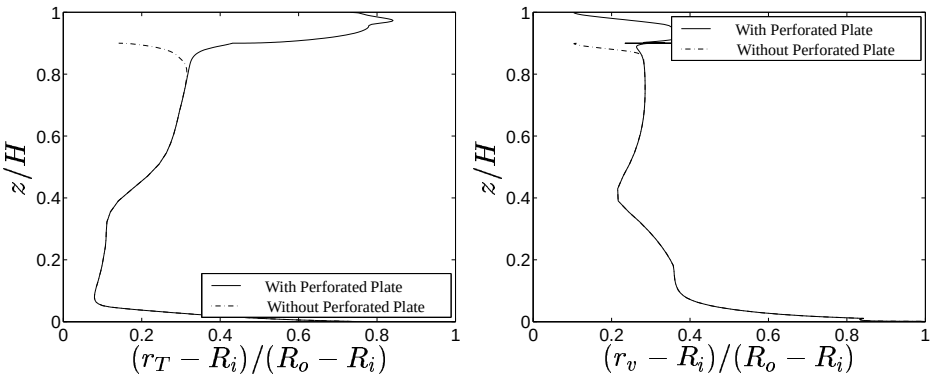

(a) thermal boundary layer (b) velocity boundary layer

Figure 10: Boundary layer growth for different geometries

Except for a very small region at the highest part of geometry, no difference between the results of the two different geometries is recognizable. This feature is still valid for the Nusselt number as it is shown in figure 11.

The grids which were used for the different geometries were 120×220 and 120×136 in r and z directions for the geometry with and without perforated plate respectively. The latter obviously, saves a great deal of computational time. Another disadvantage of having the perforated plate included in the computations is that it can create numerical problems in the future LES simulations. Also it was observed that by decreasing the grid size to 96×96 the changes in the results were less than five percent.

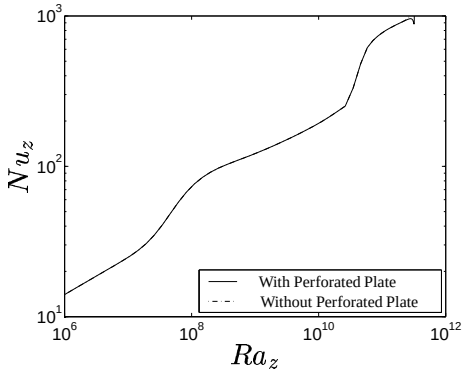

Figure 11: Heat transfer rate for different geometries

7 Effect of outlet dimension

In this section, the effect of increasing the outlet dimension is studied. When the outlet dimension is $60mm$, the flow accelerates at the outlet causing a rapid increase in Nusselt number as well as friction coefficient. As a result, high entrainment velocities (large negative v_r) will be generated near the outlet region. Whereas this is not a problem in the present 2D RANS calculations, it can introduce a problem in LES simulations, since the largest CFL number occurs in this region. This makes the LES simulations unnecessarily expensive because of the limitation of choosing small computational time steps. To overcome this problem a remedy is to increase the outlet dimension such that this increase does not affect the characteristics of fluid flow in the inner part of computational domain. Comparing different outlet boundary conditions, the results are shown in figure 12(a) and 12(b) which are in complete agreement with each other. Needless to say, the same agreement is valid for heat transfer coefficient in figure 13.

Although it is not shown here, the same agreement was achieved for an outlet with $240mm$ width. This enables us to study the flow field and heat transfer, considering hypothetical outlet dimension without expecting significant discrepancies in achieved results compared to real situation.

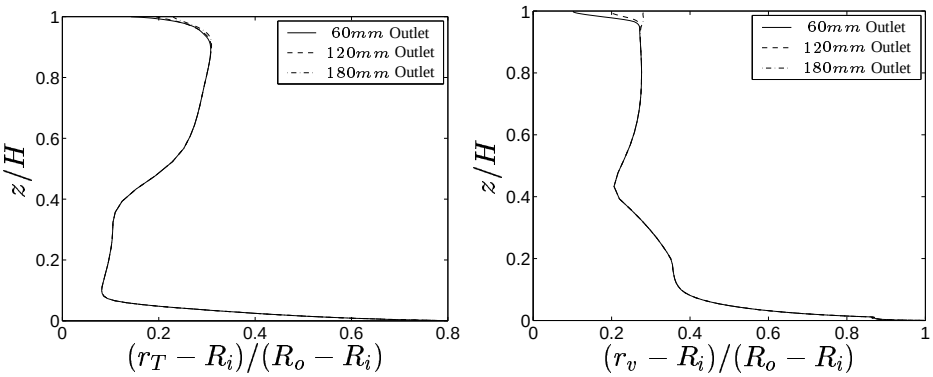

(a) thermal boundary layer (b) velocity boundary layer

Figure 12: Boundary layer growth for different outlet dimensions

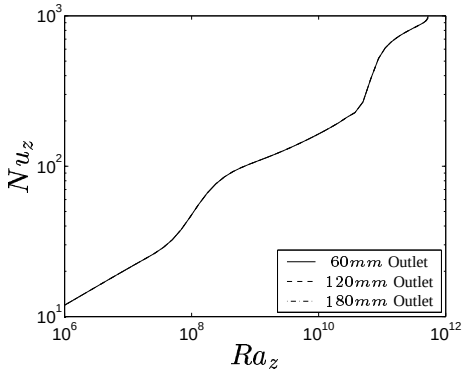

Figure 13: Heat transfer rate for different outlet dimensions

8 Effect of inlet dimension

One of the major advantages of numerical methods is that we can easily change or modify different part of the geometry in order to design, compare or anticipate the fluid and heat transfer behavior. In this study it was of particular interest to study a geometry with a doubled inlet dimension while the inlet flow rate was kept constant so that a lower initial momentum was supplied at the inlet. Figures 14(a) and 14(b) compare the thermal and velocity boundary layers growth and figure 15 compares the heat transfer rate from the heated inner tube of the two geometries. The inlet condition for the imaginary rig is adjusted such that the flow to be comparable to a real rig with $0.5m/s$ inlet air velocity.

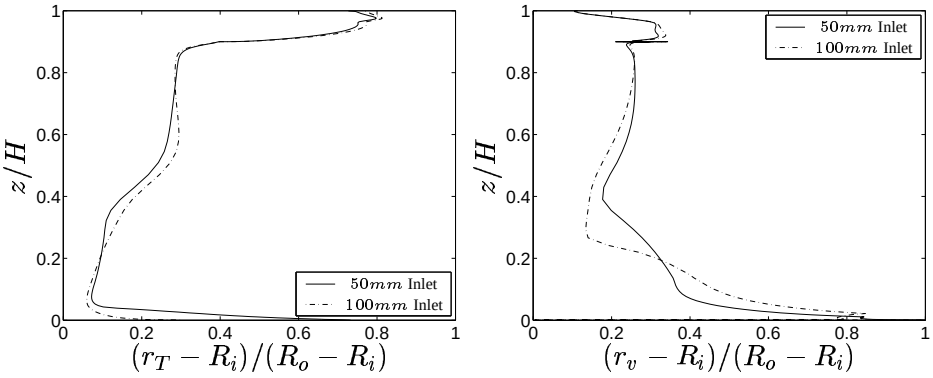

(a) thermal boundary layer

(b) velocity boundary layer

Figure 14: Boundary layer growth for different inlet dimensions

When the inlet dimension is doubled, the inlet velocity is reduced by a factor of two and as a result the transition from laminar to turbulent takes place smoother the Nusselt number increases due to fluid acceleration near the outlet. Furthermore, the commencement of transition to turbulence is sensibly retarded.

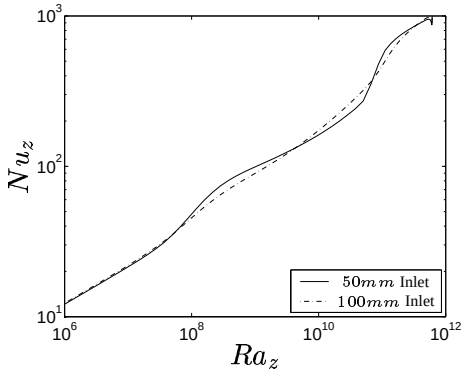

Figure 15: Heat transfer rate for different inlet dimensions

9 Effect of outer shell radius

In this section the effect of doubling the rig cross sectional area in the way that inlet flow rate to the experimental rig remains approximately constant, is investigated and the results are depicted in figures 16 and 17, in which R_{out} stands for the outer shell radius. The inlet condition for the imaginary rig is adjusted such that to be comparable to the real rig with $0.6m/s$ inlet air velocity but the mesh size and stretching factors are the same for both cases.

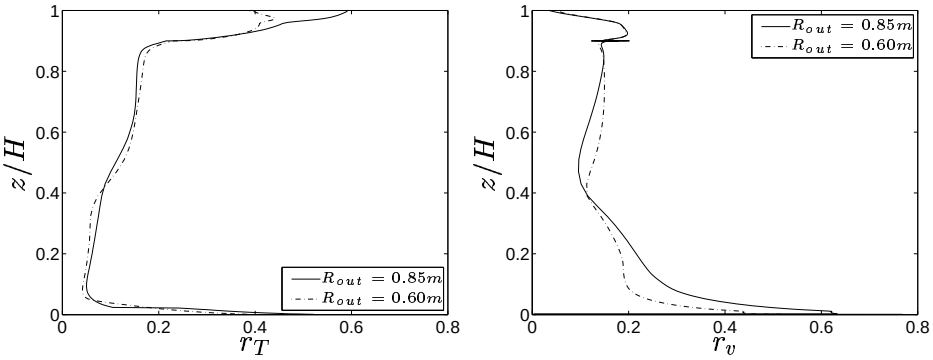

(a) thermal boundary layer

(b) velocity boundary layer

Figure 16: Boundary layer growth for different shell radii

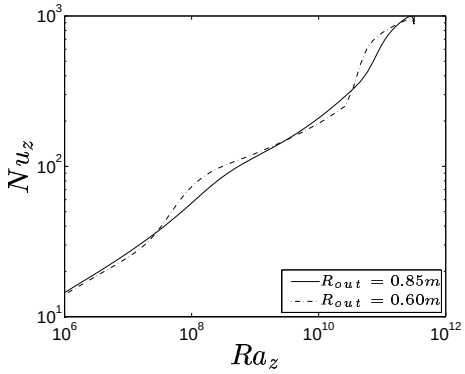

Figure 17: Heat transfer rate for different shell radii

In this case, as the geometries have different widths, the radial coordinate is not normalized. Once again, like the last case, by doubling the cross sectional area of the passing fluid, the typical velocities approximately decrease by a factor of two at the middle part of the rig. This makes the forced convection heat transfer to become less effective and consequently a smoother retarded transition occurs.

10 Conclusion

The object of the present work was to study the effect of inlet boundary conditions and geometrical parameters for a shell and tube configuration. The present work is a pre-study for a comprehensive investigation of this flow using both LES and experiment. Different inlet velocities were applied and different boundary layer growth along the heated tube were observed and it was shown that the larger the inlet velocity becomes, the larger the Nusselt number becomes. Especially near the transition region this difference is large and gradually vanishes in the fully turbulent region.

As the inclusion of the perforated plate in LES may cause some numerical problems, the effect of eliminating the plate was studied. The obtained results show that except for the very end part of the geometry no significant difference was perceived.

Having a very small outlet causes flow acceleration near the outlet. This means that in LES, a large CFL number is unavoidable. So, the

effect of outlet size on the fluid flow and heat transfer was studied and no important difference between different geometries was observed.

Because of the inlet position of the shell and tube, a large vortex at the right half of the geometry close to the shell was formed. To study its effect, one case with doubled inlet size and one with doubled shell and tube effective area cross section were investigated. In both cases the inlet flow rate was kept constant. In the former case it was found that because of smaller inlet velocity, the velocity boundary layer was thinner while no significant change in the thermal boundary layer was found showing that the mixed convection heat transfer was dominated by natural convection in both cases. However near the middle part of the shell and tube, the boundary layers were found to be thicker. This is probably due to less temperature stratification in this case. In the latter case, however, while the thermal boundary layer was not changed significantly, the velocity boundary layer became thicker near transition region. In both cases, the transition to turbulence was taken place smoother compared to the baseline case.

In figures 18(a) and 18(b) the variation of v^+ and T^+ at different Gr_z numbers for the case with $0.6m/s$ inlet velocity is compared.

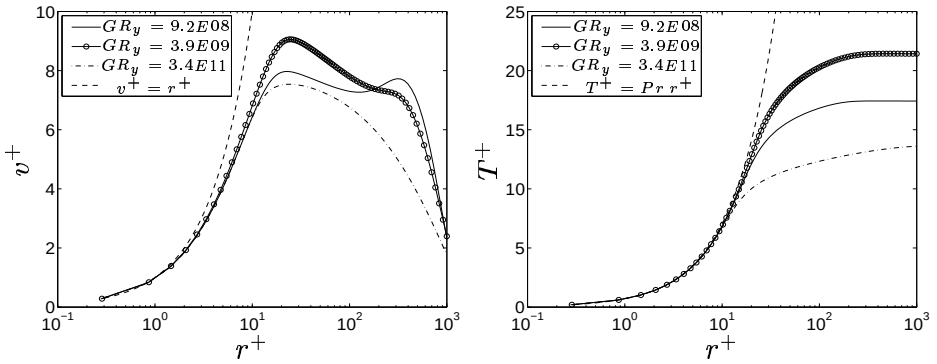

(a) Velocity profile

(b) Temperature profile

Figure 18: Velocity and temperature profiles

While in figure 18(a) it is shown that the assumption of $v^+ = r^+$ is strictly valid for $r^+ \leq 1$, in figure 18(b) the validity of $T^+ = Pr\ r^+$ for values of $r^+ \leq 5$ is shown which is in agreement with Tsuji & Nagano

(1988).

Finally, in figure 19 the amount of shell and tube energy exchange rate versus inlet velocity of the facility is shown. As it could be expected, the amount of energy consumption rate is increased with inlet velocity increase.

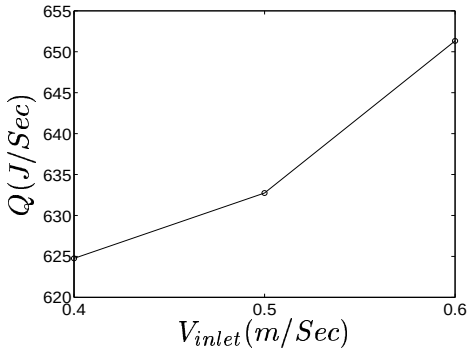

Figure 19: Energy exchange rate

Acknowledgement

This project was financed by the Swedish Research Council, project number 260-1999-354

References

ABE, K., KONDOH, T. & NAGANO, Y. 1994 A new turbulence model for predicting fluid flow and heat transfer in separating and reattaching flows - 1. Flow field calculations. *Int. J. Heat Mass Transfer* **37**, 139–151.

CHEESEWRIGHT, R. 1968 Turbulent natural convection from a plane vertical surface. *Journal of Heat Transfer* **90**, 1–8.

DAVIDSON, L. & FARHANIEH, B. 1995 CALC-BFC: A finite-volume code employing collocated variable arrangement and cartesian velocity components for computation of fluid flow and heat transfer in complex three-dimensional geometries. Rept. 95/11. Dept. of Thermo

and Fluid Dynamics, Chalmers University of Technology, Gothenburg.

MILLER, D. 1990 *Internal Flow Systems*. British Hydraulic Research Association.

PENG, S.-H. & DAVIDSON, L. 2001 Large eddy simulation for turbulent buoyant flow in a confined cavity. *International Journal of Heat and Fluid Flow* **22**, 323–331.

PENG, S.-H., DAVIDSON, L. & HOLMBERG, S. 1997 A modified low-Reynolds-number $k-\omega$ model for recirculating flows. *ASME: Journal of Fluids Engineering* **119**, 867–875.

PERSSON, N. & KARLSSON, R. 1996 Turbulent natural convection around a heated vertical slender cylinder. In *8th Int. Symp. on Applications of Laser Techniques to Fluid Mechanics*. Lisbon.

TIAN, Y. & KARAYIANNIS, T. 2000 Low turbulence natural convection in an air filled square cavity part i: the thermal and fluid flow fields. *International Journal of Heat and Mass Transfer* **43**, 849–866.

TSUJI, T. & NAGANO, Y. 1988 Characteristics of a turbulent natural convection boundary layer along a vertical flat plate. *International Journal of Heat and Mass Transfer* **31** (8), 1723–1734.

WARNER, C. & ARPACI, V. 1968 An experimental investigation of turbulent natural convection in air at low pressure along a vertival heated flat plate. *Int. J. Heat Mass Transfer* **11**, 397–406.